Homogenization of Immiscible Rubber/Rubber Polymer Mixtures by Uniaxial Compression†

Takeji Hashimoto,* Tatsuo Izumitani,‡ and Mikihito Takenaka

Department of Polymer Chemistry, Faculty of Engineering, Kyoto University, Kyoto 606, Japan. *Received October 3, 1988; Revised Manuscript Received November 22, 1988*

ABSTRACT: We explored here the molecular mechanism of the process involving mechanical mixing of immiscible polymer mixtures using polybutadiene (PB) and styrene/butadiene random copolymer (SBR) as a model system. The as-cast film, which was opaque due to the demixed structure that evolved via spinodal decomposition (SD) during the solvent evaporation, became transparent after repeated application of the uniaxial compression and exhibited no appreciable light scattering (LS). The process of the "homogenization" of the demixed structure was investigated by the laser elastic light-scattering technique. The proposed mechanism of the homogenization is as follows. Once the uniaxial compression is applied, the wavelengths (Λ's) of Fourier components of the fluctuations parallel and perpendicular to the compression axis decrease and increase, respectively. If Λ's parallel to the compression axis $\mathbf{r}_2$ are compressed to such a level that the gradient free energy of the fluctuations becomes very high, then such short-wavelength fluctuations cannot be thermodynamically stable, which results in dissolution of the fluctuations to the level appropriate for the single-phase region. The dissolution of the fluctuations along $\mathbf{r}_2$, in turn, may further cause dissolution of the Fourier components superposed to them and directed in directions other than $\mathbf{r}_2$, due to a possible coupling between the modes. The LS profile immediately after the homogenization, which was evaluated by extrapolating the time evolution of the LS profiles during the early stage SD to time zero, indicated that the homogenized mixtures have fluctuations relevant to the single-phase region near the critical point.

I. Introduction

It is well-known that polymer pairs with a high degree of polymerization, N, and a positive thermodynamic interaction parameter, χ, are not miscible to one another. Such polymer pairs can not be placed in the homogeneous state where the polymers are molecularly mixed by simple elevation of temperature. Instead of imposing the thermal energy or in addition to the thermal energy, the mechanical energy has been imposed to the mixtures in some industrial applications in order to force them into the homogeneous state.

We pursued a simple but basic study to explore the industrial mechanical mixing processes for a binary mixture of high molecular weight polybutadiene (PB) and a styrene/butadiene random copolymer (SBR) both with narrow molecular distributions. Both species are known to be rubber-like polymers. As one of the simplest modes of mechanical mixing, we applied repeated uniaxial compression and explored the change of the demixed structures involved by the compression deformation *in situ* and *at real time*.

II. Experimental Section

1. Samples. PB and SBR were polymerized by living anionic polymerization and had a narrow molecular weight distribution. SBR contains 80 wt% butadiene and has a number-average molecular weight (M_n) of 1.00×10^5 and $M_w/M_n = 1.18$ (M_w being the weight-average molecular weight). PB has $M_n = 1.6 \times 10^5$ and $M_w/M_n = 1.16$. Fractions of cis, trans, and vinyl linkages of the butadiene part as measured by infrared spectroscopy are 0.16, 0.23, and 0.61 for SBR and 0.19, 0.35, and 0.46 for PB.

2. Film Preparation. Binary mixtures of SBR/PB (70/30 v/v and 58/42 wt/wt) were dissolved into a dilute solution of toluene (7 wt % polymer solution), a mutually good solvent for PB and SBR. The 0.15-mm-thick film specimens were obtained by evaporating the solvent at a natural rate at about 25 °C in a petri dish. The as-cast films thus obtained were opaque because their internal demixed structures evolved by phase separation via the spinodal decomposition (SD) process during the solvent evaporation process (see section III-1). Some of the film specimens were *homogenized* as follows. The as-cast film was folded in two to make it twice as thick as that of the original film. The folded film was placed between the two glass plates with spacers and pressed manually to its original thickness. The homogenized film was prepared by execution of the repeated *folding–pressing* process, which occurred many times (see sections III-2 and 3), and was used as the starting material for further experiments.

3. Uniaxial Compression. The uniaxial compression was performed by the repeated folding–pressing process on the as-cast film and on the film which was first subjected to homogenization and then to isothermal demixing at 60 °C for various time intervals.[22] Depending on this time interval, the film can have various wavelengths of the dominant mode of the fluctuations formed by SD from the homogenized film. The film was compressed at 25 °C on the folded film specimens by putting a weight of 10 kg on top of the glass plates, between which the specimen was sandwiched with a spacer of an appropriate thickness. The weight was then released, and the samples were immediately used for light-scattering experiments. Generally the time scale of LS experiments is much shorter than the time scale at which the sample undergoes significant internal structure change. There was no recovery in the sample dimension after the removal of the weight. The stress relaxed completely before the implementation of the new folding–pressing process. The complete stress relaxation took place for a few minutes.

4. Method of Observations. The change of the demixed structure with the implementation of uniaxial compression was investigated in situ and each time by observing elastic light-scattering patterns. He–Ne laser of 15-mW power was used as an incident beam source, and the light scattering (LS) was observed photographically or photometrically by sending incident beam parallel to the compression axis. Thus, the small-angle LS patterns to be studied here reflect essentially the Fourier mode of the fluctuations nearly parallel to the film surface.

III. Experimental Results and Discussion

1. Miscibility of Mixtures and Structure in As-Cast Films: "Structure Memory" in Solution. The two polymers turned out to be so immiscible that the cloud points of the mixtures were very high and could not be directly measured by a simple elevation of temperature without the influence of thermal degradation. The cloud points were thus measured by introducing a nonvolatile and neutral solvent, e.g., dioctyl phthalate (DOP), and by

† Presented at the 35th Annual Polymer Symposium, Society of Polymer Science Japan, Osaka University, Nov 1986 (Izumitani, T.; Takenaka, M.; Hashimoto, T. *Polym. Prepr. Jpn., Soc. Polym. Sci. Jpn.* **1986**, *35*, 2974).

‡ On leave from Research Center, Daicel Chemical Industries, Ltd., 1239, Shinzaike, Aboshi-ku, Himeji, Hyogo 671-12, Japan.

0024-9297/89/2222-2293$01.50/0

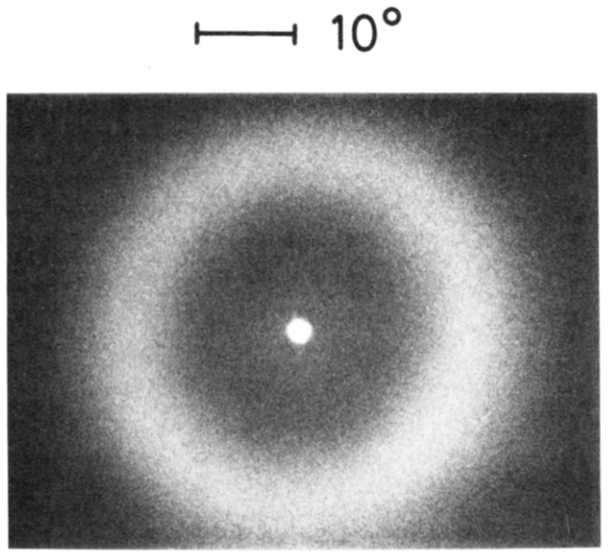

Figure 1. Light-scattering pattern showing spinodal ring for the as-cast film for SBR/PB = 70/30 v/v. The angle mark corresponds to a scattering angle θ equal to 10° in air.

extrapolating the cloud points to zero solvent concentration, although the extrapolation process may not necessarily be valid, especially when the phase diagram of the bulk mixture has the hourglass-type character. The cloud points determined this way were as high as 400–450 °C for the near critical mixtures.[7] The critical composition exists at volume fraction of SBR of $\phi_{SBR} \simeq 0.7$.

Figure 1 shows a typical LS pattern observed for the as-cast films. The pattern has a scattering maximum at a magnitude of scattering vector $|\mathbf{q}| = q_m$,

$$|\mathbf{q}| = (4\pi/\lambda) \sin(\theta/2) = q_m \simeq 2.7 \times 10^4 \text{ cm}^{-1} \quad (1)$$

corresponding to a spacing Λ_m of 2.3 μm where

$$\Lambda_m = 2\pi/q_m \quad (2)$$

In the first line of eq 1, λ and θ are, respectively, the wavelength of light and the scattering angle in the medium. The scattering maximum reflects very basic aspects of structure formation in the solution.[1,2]

The previously established picture[1,2] for the structure evolution during the solvent evaporation is expected to be applicable to this system. During the solvent evaporation process, the concentration of the solution increases, and the demixing starts to occur between PB solution and SBR solution according to the SD mechanism, since the solvent is nonselective for both polymers. The SD will develop a periodic concentration fluctuation with wavenumber q_m. During the solvent evaporation process, the fluctuations will grow in size and in amplitude, resulting in the fluctuations observed in the bulk film.

Thus, the scattering maximum in bulk as-cast films reflects the spatial concentration fluctuations built up in the solution by the SD and subsequent coarsening process[4,5] during the solvent evaporation process and therefore the *structure memory* in the solution. The memory was confirmed directly by real-time observation of light-scattering profiles during demixing of the solutions at given temperatures and concentrations for polystyrene (PS)/PB/toluene (Tol) and for PS/PS–PB diblock polymer (SB)/Tol systems.[1] A similar memory effect was also presented by Inoue et al.[2]

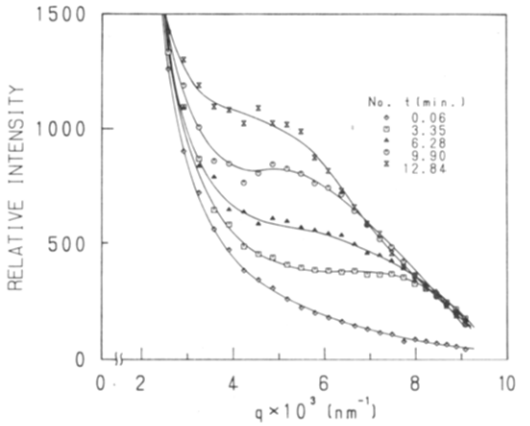

Figure 2. Time-sliced light-scattering profiles measured during isothermal phase separation at 84.0 °C for DOP solution of SBR/PB = 75/25 wt/wt with total polymer concentration of 30 vol %. The cloud point of the solution is 90.7 °C.

Figure 2 shows typical results of time evolution of LS profiles measured by a time-resolved LS apparatus[3] after quenching the ternary mixture of PB/SBR/DOP from the homogeneous state, i.e., 121.0 °C, to the phase separation temperature, 84.0 °C, which corresponds to the temperature inside the spinodal-phase boundary. The ternary mixture contains 30 vol % total polymers, i.e., SBR and PB. SBR content in the polymer mixtures is 70 vol % and has a cloud point at 90.7 °C. During the isothermal demixing at 84.0 °C, the scattering maximum appears shortly after the demixing. As the demixing progresses, the intensity increases and the scattering maximum shifts toward smaller angles, indicating that the demixing involves an increase of the wavelength and amplitude of the periodic concentration fluctuations. The change of the scattering profiles with time corresponds to the late stage of SD[4,5] for this particular case. It should be noted that the increase in intensity with decreasing q in the small q regime ($q < 2.0 \times 10^{-3}$ nm^{-1}) may be a consequence of increased parasitic scattering with decreasing q or increased contribution of the concentration fluctuations between polymers and solvent. The structure evolution during the solvent evaporation is an athermal process and hence is more complicated than that involved by this isothermal demixing process. Yet they should have a common fundamental feature. The entire SD process for a critical mixture has been qualitatively classified into three regimes:[6] (i) the *early stage SD*, (ii) the *intermediate stage SD*, and (iii) the *late stage SD*. In the early stage SD, the wavelength, Λ_m, of the dominant mode of the fluctuations is essentially constant with time, and the amplitude of the fluctuation, $\Delta\phi$, increases exponentially with time. This unique feature results from the weakly nonlinear nature of the early stage SD process. The early stage SD from the "homogenized" mixture was discussed previously.[7,8] In the intermediate stage, the nonlinear nature of the demixing process becomes important, causing coarsening processes, and therefore increases in both Λ_m and $\Delta\phi$ with time. In the late stage, $\Delta\phi$ reaches an equilibrium value, $\Delta\phi_e$, and only the wavelength increases. Here the dynamical scaling hypothesis[10,11] becomes valid, and the dynamical self-similarity should exist in structure evolution.[10,11] The as-cast film and the film employed for the subsequent uniaxial compressions in this study have demixed structures corresponding to the intermediate stage or in most of the cases to the late stage, as described in a subsequent paper.[9]

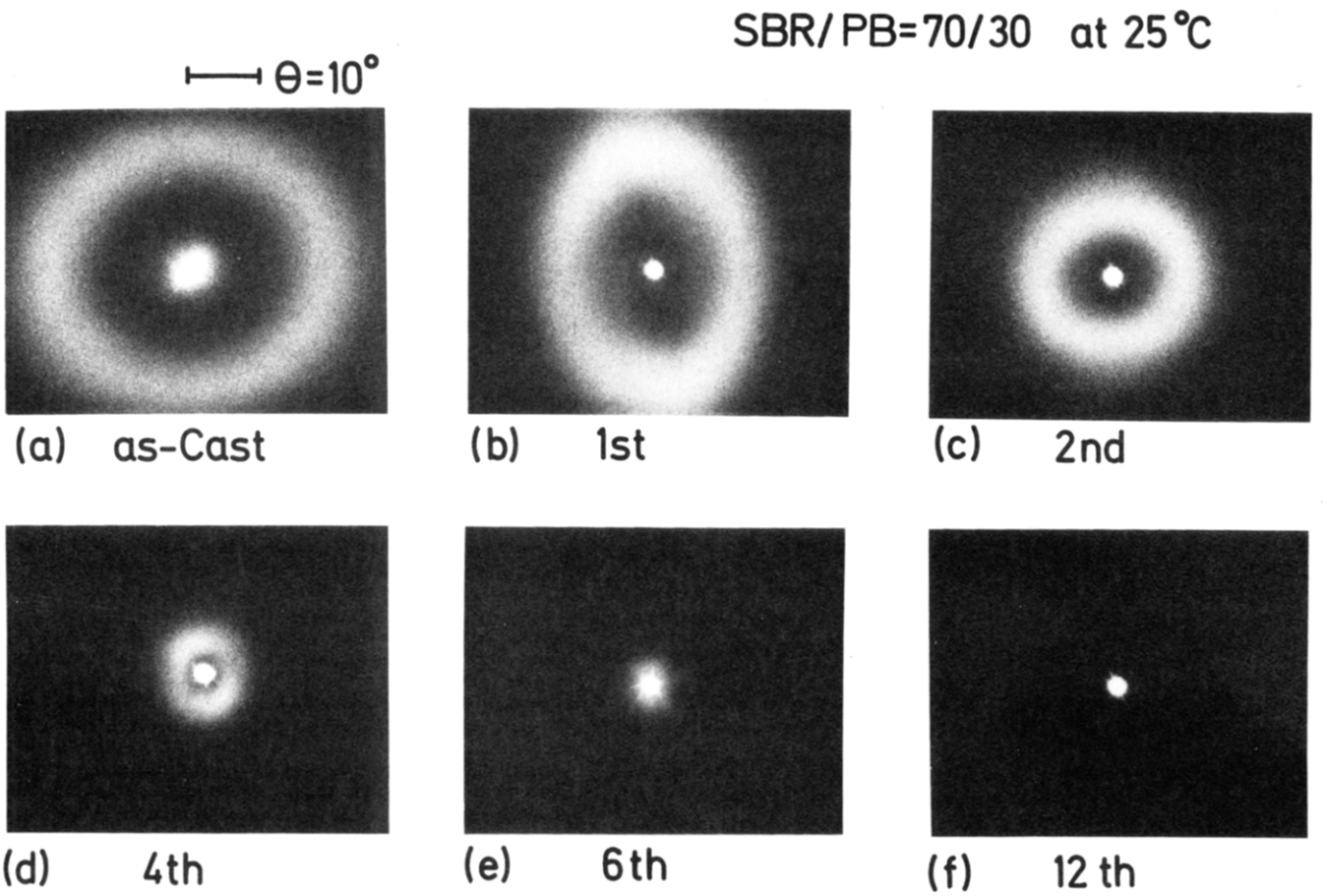

Figure 3. Light-scattering pattern for the as-cast film (a) and the change of the pattern with a number of repeats (n) of the $^1/_2$ compression. Patterns b–f correspond to n = 1, 2, 4, 6, and 12, respectively. The angle mark for θ has the same meaning as in Figure 1. SBR/PB = 30/70 v/v.

2. Uniaxial Compression and Change of Demixed Structures. Figure 3 shows LS patterns observed at 25 °C for the as-cast film of the SBR/PB mixture (part a) and the change of the patterns with the uniaxial compressions (parts b–f). The film specimen was folded in two and pressed uniaxially into the original film thickness. The process will be designated as "$^1/_2$ compression", and each time, the LS pattern was observed according to the manner as described in section II-3. Patterns b–f in Figure 3 represent, respectively, those after implementation of the $^1/_2$ compression by 1, 2, 4, and 6, and 12 times.

Upon repetition of the $^1/_2$ compression, the "spinodal ring", i.e., the scattering maximum arising from a periodic concentration fluctuation in space which was developed by SD, shifts toward a smaller scattering angle and finally disappears. Pattern f shows the transmitted incident beam alone. The weak residual scattering in pattern f, which turned out to have an intensity level relevant to the critical fluctuations of the mixture in the single-phase near critical point (see section III-3), is not detectable by the photographic method. Detailed analyses (section III-3) indicated that the disappearance of the spinodal ring is indicative of the homogenization. The distortion of the ring from the circle to the ellipse is due to a shear deformation. The change of the spacing with n repetitions of the $^1/_2$ compression for the as-cast film is included in Figure 8 (solid circles) where Λ_0 and Λ_n are, respectively, the spacings for the undeformed film and the film subjected to the compression n times.

The $^1/_2$ compression was implemented to the film in a few minutes. This time scale is much shorter than that for the structural evolution driven by the thermodynamic force but is longer than that for stress relaxation and hence for the relaxation of molecular orientation. Figure 4 shows the stress relaxation at 41.8 °C after shear strain was applied to the mixture subjected first to homogenization and followed by phase separation for 1 h at 75 °C. The findings indicate a significant fraction of stress decay in 1 min. Therefore the stress and molecular orientation are relaxed each time before a new $^1/_2$ compression is implemented to the specimens. However, the time scale of the successive $^1/_2$ compression (about 3 min) is short enough not to permit a significant growth of the concentration fluctuations, which causes a cumulative deformation effect on the

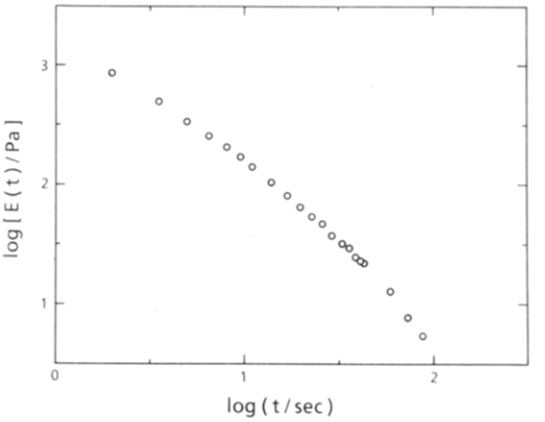

Figure 4. Stress relaxation of SBR/PB = 70/30 v/v at 41.8 °C where the shear modulus, $G(t)$, was plotted as a function of time, t, in second. The mixture was first homogenized and then phase separated at 75 °C for 1 h. The shear strain was 1.85.

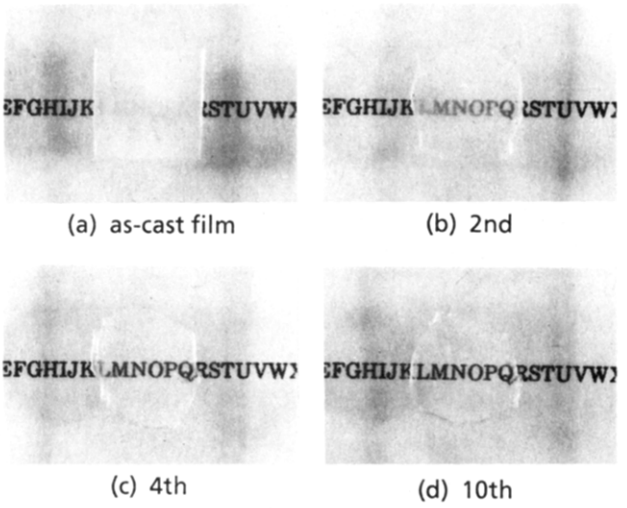

Figure 5. Transparency of the as-cast film (a) and the film subjected to the $^1/_2$ compression n times; (b) $n = 2$, (c) $n = 4$, and (d) $n = 10$. SBR/PB = 70/30 v/v.

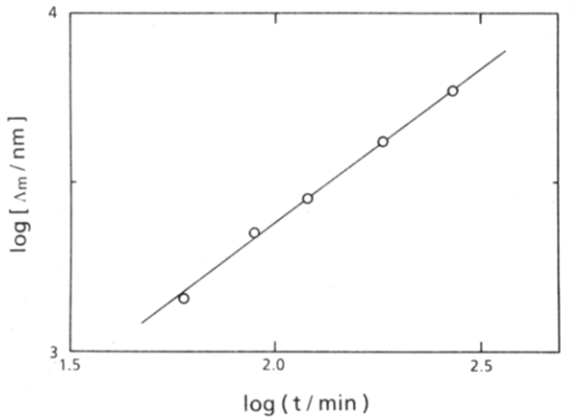

Figure 6. Change of the wavelength Λ_0 of the dominant mode of the concentration fluctuations for the film that was first homogenized and then phase separated by annealing for a given time period, t, at 60 °C.

initially existing, phase-separated domain structure.

Figure 5 intuitively demonstrates that the clarity of the sample specimen improves with an increasing number of $^1/_2$ compressions. Here the same sample specimen was used, and the specimen after the compression had the same sample thickness.

The compression experiment was carried out also by systematically changing the initial condition for the demixed state. For this purpose, the as-cast film was first homogenized in the manner as discussed in connection with Figure 3, by implementing the compression at least 20 times and then by annealing at 60 °C for various times, typically 1–4.5 h to allow phase separation to various demixed states. The spacing Λ_0's for the undeformed specimens as prepared by this method vary from 1.5 to 5.9 μm as shown in Figure 6. All the undeformed specimens have definitely periodic and bicontinuous domain structures relevant to the late stage SD where the dynamical scaling and self-similarity are observed in the time evolution of the structure.[9]

Figure 7 shows a typical spinodal ring for the annealed film (at 60 °C for 1.5 h) after homogenization (part a) and its change with the repetition of the $^1/_2$ compression at 25 °C (parts b–d). The annealed film has $\Lambda_0 = 2.2$ μm. Essentially the same phenomenon as that observed for the as-cast film was observed here. The spacing after applying the $^1/_2$ compression n times (Λ_n) can be determined from the scattering angle ($\theta_{\max,n}$) or the scattering vector ($\mathbf{q}_{\max,n}$) of the corresponding ring-scattering maximum,

$$\Lambda_n = 2\pi/|\mathbf{q}_{\max,n}| \qquad |\mathbf{q}_{\max,n}| = (4\pi/\lambda)\sin(\theta_{\max,n}/2) \quad (3)$$

Figure 8 shows the change of Λ_n relative to the initial wavelength Λ_0 plotted as a function of n for the annealed films with various values of Λ_0's. If the change of Λ_n with the uniaxial compression obeys *isochoric affine deformation*, we should have

$$\Lambda_n/\Lambda_0 = 2^{n/2} \quad (4)$$

This prediction was drawn by a straight line of slope (1/2) log 2 in Figure 8. The change of Λ_n/Λ_0 with n and therefore the deformation as observed in the direction perpendicular to the compression axis seem to be universal and independent of Λ_0. The expansion of the spacing normal to the compression axis seems to be greater than that predicted by the affine deformation. This may be due to the fact that the uniaxial compression involves such a constrained deformation that the interfaces between the rubber specimen and the glass are essentially fixed, no slippage taking place at the boundary.

It is also very important to note that the scattering intensity appears to become weak with increasing n, especially $n \gtrsim 3$ as indicated in Figure 7d. Now let us define the components of the scattering vector ($\mathbf{q}$) and those of the wavelength of the dominant mode of the concentration fluctuations parallel and perpendicular to the compression axis as ($q_\parallel$, $q_\perp$) and ($\Lambda_\parallel$, $\Lambda_\perp$), respectively; then the scattered intensity is generally given by

$$I(\mathbf{q}) = I(q_\parallel, q_\perp) = \langle\eta^2\rangle\Lambda_\perp{}^2\Lambda_\parallel S(q_\parallel\Lambda_\parallel, q_\perp\Lambda_\perp) \quad (5a)$$

where $\langle\eta^2\rangle$ is the mean-squared fluctuation of the refractive index which is related to the mean-squared fluctuation in the amplitude of the concentration fluctuation of one component. S is a scaling function which changes in general between unity and zero with changing $\mathbf{q} = (q_\parallel, q_\perp)$. The simple isochoric affine deformation that the rubberlike materials should obey with good approximation demands that $\Lambda_\perp{}^2\Lambda_\parallel = \Lambda_0{}^3$ constant, independent of n. Thus, the decrease of the peak intensity as seen in Figure 7d is a consequence of the decrease of $\langle\eta^2\rangle$, which suggests that the repetitive compression involves dissolution of the concentration fluctuations, i.e., the mechanism which cannot be explained by the simple affine deformation. Here it should be noted that the scattering intensity shown in the patterns of Figures 3 and 7 corresponds to

$$I(q_\perp) \equiv I(q_\parallel{=}0, q_\perp) = \langle\eta^2\rangle\Lambda_\perp{}^2\Lambda_\parallel S(q_\perp\Lambda_\perp) \quad (5b)$$

The change of the scattering profile with the $^1/_2$ compression may be studied more quantitatively by scanning the intensity with a photomultiplier. Figure 9 shows some typical results, where parts a and b show, respectively, the results for the films prepared by annealing the homogenized films of 58/42 wt/wt SBR/PB at 60 °C for 0.5 and 1 h. The profiles marked with $n = 0$, 1, 2, 3, 4, and H represent, respectively, those for as-annealed film, the film subjected to the $^1/_2$ compression over 1, 2, 3, and 4 times, and the homogenized film. The observed shifts of the peak positions with compression obey the rule on the spacing change given by Figure 8. The arrow marked $n = 3$ in part a and the arrow marked $n = 4$ in part b correspond to the peak positions expected from the result given by Figure 8. We interpret here that the peaks $n = 3$ (in part a) and 4 (in part b) are buried in the zeroth-order scattering. The profile for the homogenized film corresponds to that given by Figure 13a.

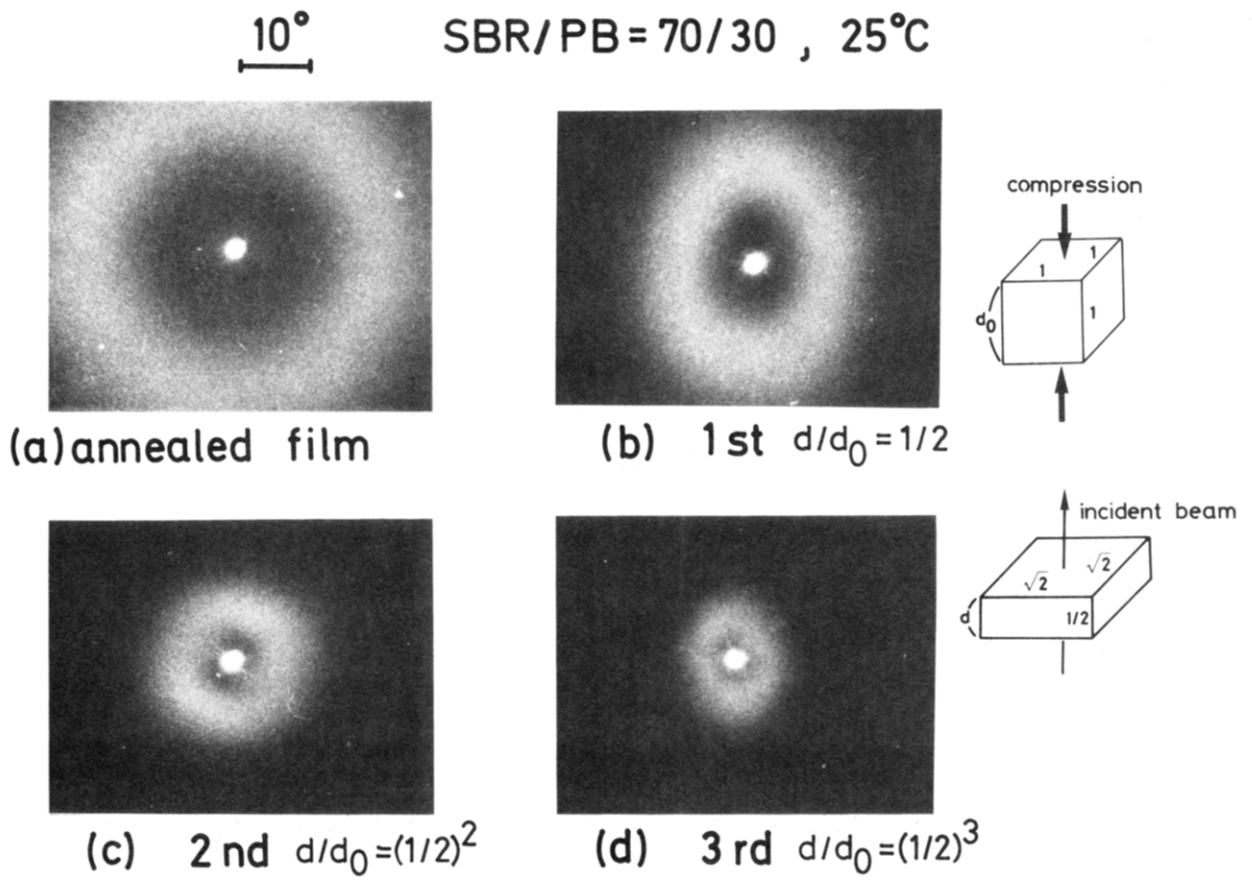

Figure 7. Light-scattering pattern for the film that was first homogenized and then phase separated by annealing for 1.5 h at 60 °C (a) and its change with a uniaxial compression n times; n = 1 (b), 2 (c), and 3 (d). The angle mark for θ has the same meaning as in Figure 1. SBR/PB = 70/30 v/v.

The isochoric affine deformation predicts that the measured scattered intensity profiles, $I(q_\perp)$, should be universal and superposable to each other if I is plotted as a function of the reduced scattering vector, $q_\perp\Lambda_\perp = q_\perp/q_{\perp,max}$, since $\langle\eta^2\rangle\Lambda_\perp{}^2\Lambda_\parallel$ should be constant in eq 5b. Here $q_{\perp,max}$ is the peak position. However, they are not superposable as the peak intensity increases by increasing n from 0 to 1. The peak intensity decreases by increasing n from 2 to 3 in part a and from 2 to 4 in part b, where the peaks for n = 4 (in part a) and n = 3 (in part b) may be buried in the respective zeroth-order peak. They are not superposable also from the viewpoint that the profile itself is changing by increasing n from 2 to 3 in part a and from 3 to 4 in part b. Thus, the deformation involves some processes beyond the single affine deformation. The decrease of the peak intensity is expected to result essentially from the decrease of $\langle\eta^2\rangle$, which, in turn, results from the dissolution of the fluctuations $\eta_{\mathbf{q}}$'s with $\mathbf{q}$ higher than q_c during the compression process. Here $\eta_{\mathbf{q}}$ is the amplitude of the $\mathbf{q}$-Fourier mode of the spatial refractive index fluctuation $\eta(\mathbf{r})$:

$$\eta(\mathbf{r}) = \sum_{\mathbf{q}} \eta_{\mathbf{q}} \exp[i(\mathbf{r}\cdot\mathbf{q})] \tag{6a}$$

The mean-squared fluctuations, $\langle\eta^2\rangle$, related to the peak intensity are given by

$$\langle\eta^2\rangle = \sum_{\mathbf{q}} \eta_{\mathbf{q}}{}^2 \tag{6b}$$

Consequently, the increasing dissolution of the modes with the number of compressions, n, causes a decrease of $\langle\eta^2\rangle$ and hence the peak intensity. The increase of the fluctuations with the first compression may imply generation of the new fluctuations by the first compression process.

The change of the spatial concentration fluctuations with the $^1/_2$ compression was also observed in real space. Figure 10 shows typical photographs of the effect of the $^1/_2$ compression for the as-cast film on the periodic bicontinuous structure as observed by optical microscopy. With the increase in the number, n, of the repeated compressions (e.g., from n = 1 to 4), the spacing Λ_n is observed to increase, which is in accord with the LS observations. Simultaneously, the contrast between the coexisting two phases tends to be lost rapidly with increasing n, only a faint contrast being discernible for $n \gtrsim 4$. This observation is believed to reflect the significant decrease of LS intensity for the specimens subjected to compression more than 3 times (Figures 7d and 9). Finally, picture f obtained after compression over 12 times exhibits no remarkable structure, a uniform structure being attained at least in the microscopic scale.

3. Stability of Homogenized Structure. Here we attempt to analyze the spatial concentration fluctuations that exist in the homogenized state. However, we should note that the homogenized state is *stable only under the external mechanical excitation.* Once the external mechanical field is stopped, the homogenized state becomes immediately *unstable* and hence undergoes spinodal decomposition. To understand the homogenization mechanism, it is important to note that the growth rates, $R(q)$, for the concentration fluctuations with wavevector q are all extremely slow, much slower than the rate of the applied deformation, as shown later and as described elsewhere.[7,8] Thus, no significant growth of the fluctuations can essentially occur during the uniaxial compression, which, in turn, would imply that the *applied deformation is cummulatively effective* for the homogenization.

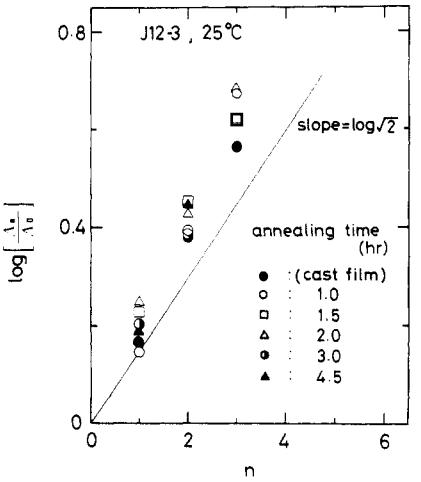

Figure 8. Change of the wavelength Λ_n of the dominant mode of the concentration fluctuations for the film subjected to the $^1/_2$ compression n times. The films were first homogenized and then phase separated by annealing at 60 °C for various time periods and hence have various values of Λ_0 for the wavelengths before the compression.

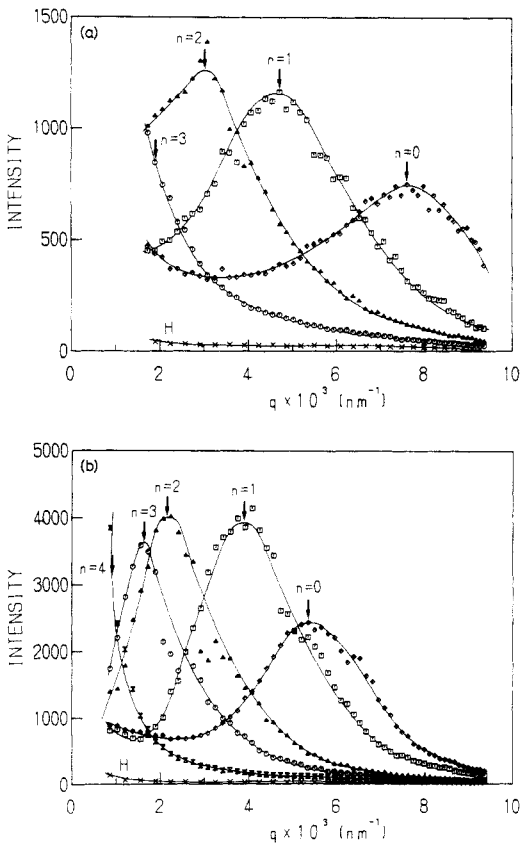

Figure 9. Light-scattering profiles for the as-annealed films (n = 0), for the film subjected to the $^1/_2$ compression n times (n = 0, 1, 2, and 3 (a) and n = 0, 1, 2, 3, and 4 (b)), and for the film subjected to the homogenization (H). SBR/PB = 58/42 wt/wt. The film was homogenized and subsequently annealed for 0.5 and 1 h.

Figure 11 shows typical time evolution of light-scattering patterns at 30 °C from the homogenized film (c–f), as well as the patterns for the as-cast film (a) and immediately after the homogenization (b). As is well expected, the homogenized mixture does undergo spinodal decomposition at 30 °C after stopping the repeated uniaxial compression. Patterns c–f, which show the shift of the peak position toward smaller scattering angles and increasing peak intensity with time, reflect the time evolution of the percolated and phase-separated structure during the late stage spinodal decomposition with a very slow growth rate.[9]

By use of the time-resolved light-scattering method with a photomultiplier,[3] the evolution of light-scattering profiles from the homogenized film, which were not detectable by the photographic light-scattering method, was quantitatively investigated immediately after mixing up to about 1 h. The results indicated that the time evolution of light-scattering profiles in the early stage unmixing process can be described with good accuracy by the linearized theory of the spinodal decomposition.[7,8]

Figure 12 shows the time evolution of light-scattering profiles in the early stage spinodal decomposition for the 58/42 wt/wt SBR/PB mixture at 40 °C from the homogenized film prepared by repeated uniaxial compression at 40 °C. Part a of Figure 12 shows time-sliced light-scattering intensity (I) as a function of q, and part b shows logarithms of the scattered intensity as a function of time after the homogenization at various q's. As shown in the figure, the scattering shortly after the homogenization is very weak, but the intensity grows exponentially with time at growth rate $R(q)$ depending on q, $R(q)$ being maximum at $q = q_m \cong 1.0 \times 10^{-2}$ nm^{-1}. The Cahn–Hilliard–Cook theory[12,13] on the early stage spinodal decomposition predicts that the time evolution of the scattered intensity, $I(q, t)$, is given by

$$I(q, t) = I_T(q) + [I(q, t=0) - I_T(q)] \exp[2R(q)t] \quad (7)$$

where $I_T(q)$ is the virtual structure factor[14,15] at the phase separation temperature T, e.g., 40 °C in the case of Figure 12, and $I(q, t=0)$ is the initial scattered intensity before the phase separation, e.g., the scattered intensity right after the homogenization.

As shown immediately below, the homogenized state turned out to be a state where the mixture is in a single-phase state near the critical point, but the mixture is far from the critical point and hence is in deep quench at the phase separation temperature. Under this condition, it is well expected that

$$I(q, t=0) \gg |I_T(q)| \quad (8)$$

The random thermal noise $|I_T(q)|$ does not play a significant role for $I(q, t)$, so we expect the exponential growth as observed in the experiments to be

$$I(q, t) = I(q, t=0) \exp[2R(q)t] \quad (9)$$

Thus, in this case, one can estimate $I(q, t=0)$ corresponding to the scattering profile immediately after the homogenization and before the phase separation by extrapolating the linear part in the plot ln $I(q, t)$ versus t to time zero.

4. Analyses of the Homogenized State. In Figures 13a and 14a, $I(q, t=0)$'s thus determined are defined as $I_s(q)$ and are shown by open circles. Figures 13b and 14b show the Ornstein–Zernike (OZ) plots, i.e., $I_s(q)^{-1}$ versus q^2. The experimental results are in good agreement with the OZ formula[19,20]

$$I_s(q) = I_s(0)/[1 + q^2\xi^2] \quad (10)$$

which implies that the scattering reflects the critical fluctuation in the single-phase state.[16] The best fits with the OZ formula are shown by solid lines in Figures 13 and 14 and yield the correlation length ξ = 160 nm for the mixture 58/42 wt/wt SBR/PB (Figure 13) and 98 nm for the mixture 25/75 wt/wt SBR/PB (Figure 14). Since the gyration radius, $R_{g,PB}$, of the unperturbed PB is expected to be 19 nm, the correlation lengths ξ = 160 and 98 nm are about $9R_{g,PB}$ and $5R_{g,PB}$, respectively, very large compared with the size of the individual coils. This further implies that *the homogenized state corresponds to the single-*

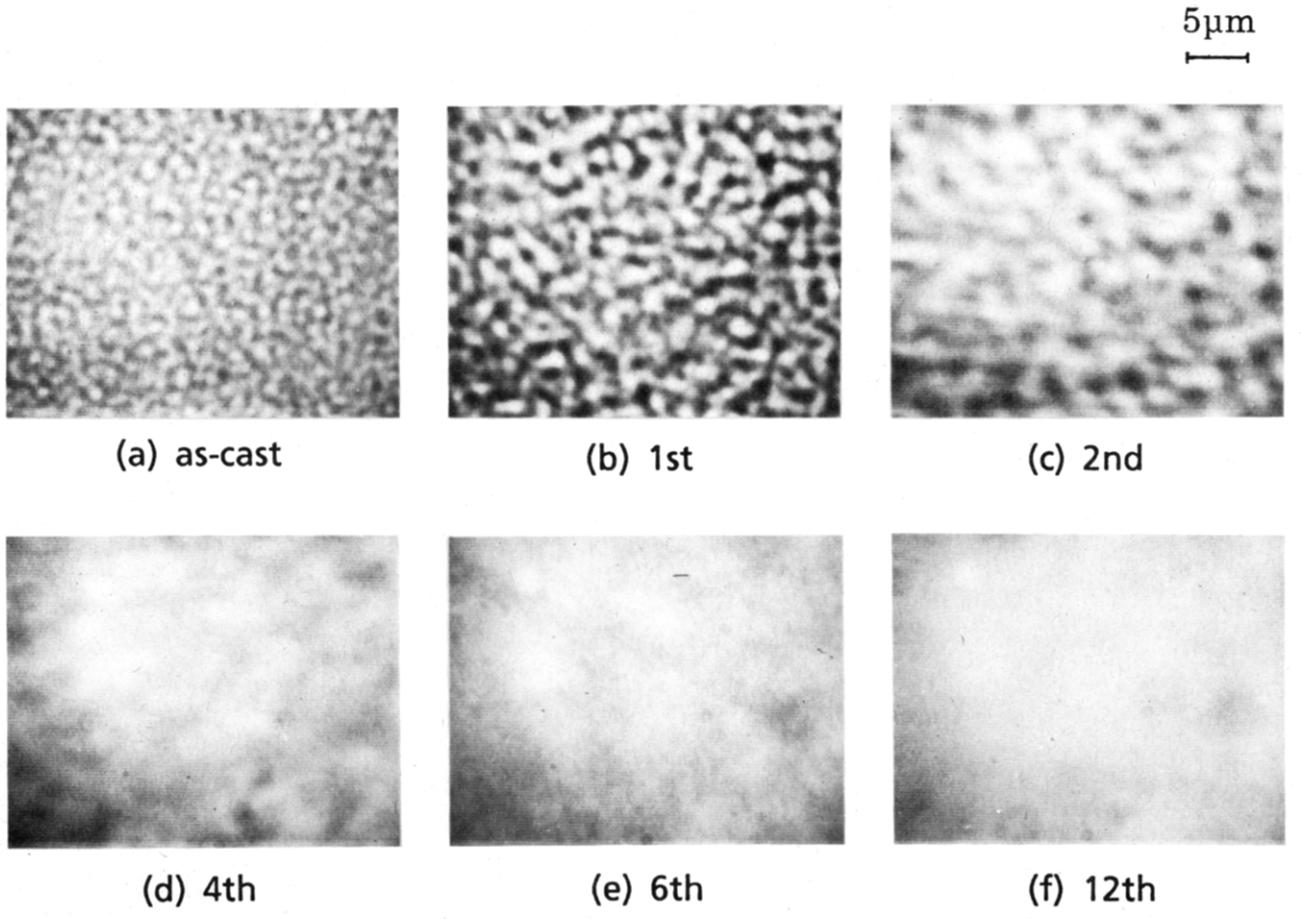

Figure 10. Spatial concentration fluctuations of as-cast film of 70/30 v/v SBR/PB as observed under optical microscope and its change with the repetition of the $^1/_2$ compression n times. n = 1 (b), 2 (c), 4 (d), 6 (e), and 12 (f).

phase state near the critical point and has large scattered intensity $I_s(q)$ or $I(q, t=0)$ as discussed above in connection with eq 7 and 8.

Now the correlation length, ξ, in the OZ equation for the mixtures which contain a random copolymer as one component have the properties discussed below. The scattering function for such mixtures in the single-phase state is given by[17]

$$\left[\frac{I(q)}{(a-b)_{\text{eff}}^2}\right]^{-1} = \frac{1}{\phi_{\text{PB}}N_{\text{PB}}g(q;N_{\text{PB}})} + \frac{1}{(1-\phi_{\text{PB}})N_{\text{SBR}}g(q;N_{\text{SBR}})} - 2\chi_{\text{eff}} \quad (11)$$

based on the mean-field random phase approximation,[16] where

$$\chi_{\text{eff}} = \chi(1-\psi)^2 \quad (12)$$

$$(a-b)_{\text{eff}}^2 = (a-b)^2(1-\psi)^2 \quad (13)$$

Here ϕ_{PB} is the volume fraction of PB in the SBR/PB mixture, N_{PB} and N_{SBR} are the polymerization indexes of PB and SBR, and $g(x)$ is the Debye function,

$$g(x) = (2/x^2)[x - 1 + \exp(-x)] \quad (14)$$

$$x = q^2R_g^2 \quad (15)$$

and $x_{\text{PB}} = q^2R_{g,\text{PB}}^2$ and $x_{\text{SBR}} = q^2R_{g,\text{SBR}}^2$. $R_{g,\text{PB}}$ and $R_{g,\text{PB}}$ are the gyration radii of unperturbed chains for PB and SBR, respectively, and χ is the Flory interaction parameter per monomer between PB and polystyrene (PS). ψ is a fraction of butadiene monomer in SBR. a and b are the scattering contrasts (i.e., refractive indexes in the case of LS) for pure PB and PS, respectively. For the small-q region satisfying $qR_g \ll 1$, as in our case, one can expand $g(x)$ in eq 11 into a series of x and obtain the OZ formula given by eq 10, where ξ is given by

$$\xi^{-2} = 36\phi_{\text{PB}}(1-\phi_{\text{PB}})(\chi_s - \chi_{\text{eff}})/l^2 \quad (16)$$

where l is the Kuhn statistical segment length, and χ_s is given by

$$2\chi_s = (\phi_{\text{PB}}N_{\text{PB}})^{-1} + (1-\phi_{\text{PB}})^{-1}N_{\text{SBR}}^{-1} \quad (17)$$

χ_s is the χ parameter at the spinodal point.

From the estimated value of ξ together with information on ϕ_{PB}, N_{PB}, and N_{SBR}, one can estimate $(\chi_s - \chi_{\text{eff}})/\chi_s \equiv \epsilon_T$, a parameter describing a state of the homogenized mixture. If $\epsilon_T \ll 1$, the homogenized mixture corresponds to a mixture in the single phase very near the critical point. On the other hand, if $\epsilon_T \cong 1$, the homogenized mixture corresponds to a thermodynamically very stable mixture in the single phase, very far from the critical point. By use of $R_{g,\text{PB}}$ = 18 nm and the weight-average degrees of polymerization of $N_{\text{PB}} = 3.54 \times 10^3$ and $N_{\text{SBR}} = 1.97 \times 10^3$, one obtains $\epsilon_T \cong 3 \times 10^{-3}$ for the mixture 58/42 wt/wt SBR/PB and $\epsilon_T \cong 7 \times 10^{-3}$ for the mixture 25/75 wt/wt SBR/PB. Thus, the homogenized states correspond to the single-phase state very near the critical point.

On the basis of eq 12, one can estimate χ_{eff} at the phase separation temperature (40 or 60 °C) to be about 10^{-3} by inserting $\chi \cong 0.1$[8,18] and $\psi = 0.8$. Thus, the parameter $\epsilon_T = (\chi_{\text{eff}} - \chi_s)/\chi_s$ associated with the quench depth of the mixture in the two-phase region can be estimated to be

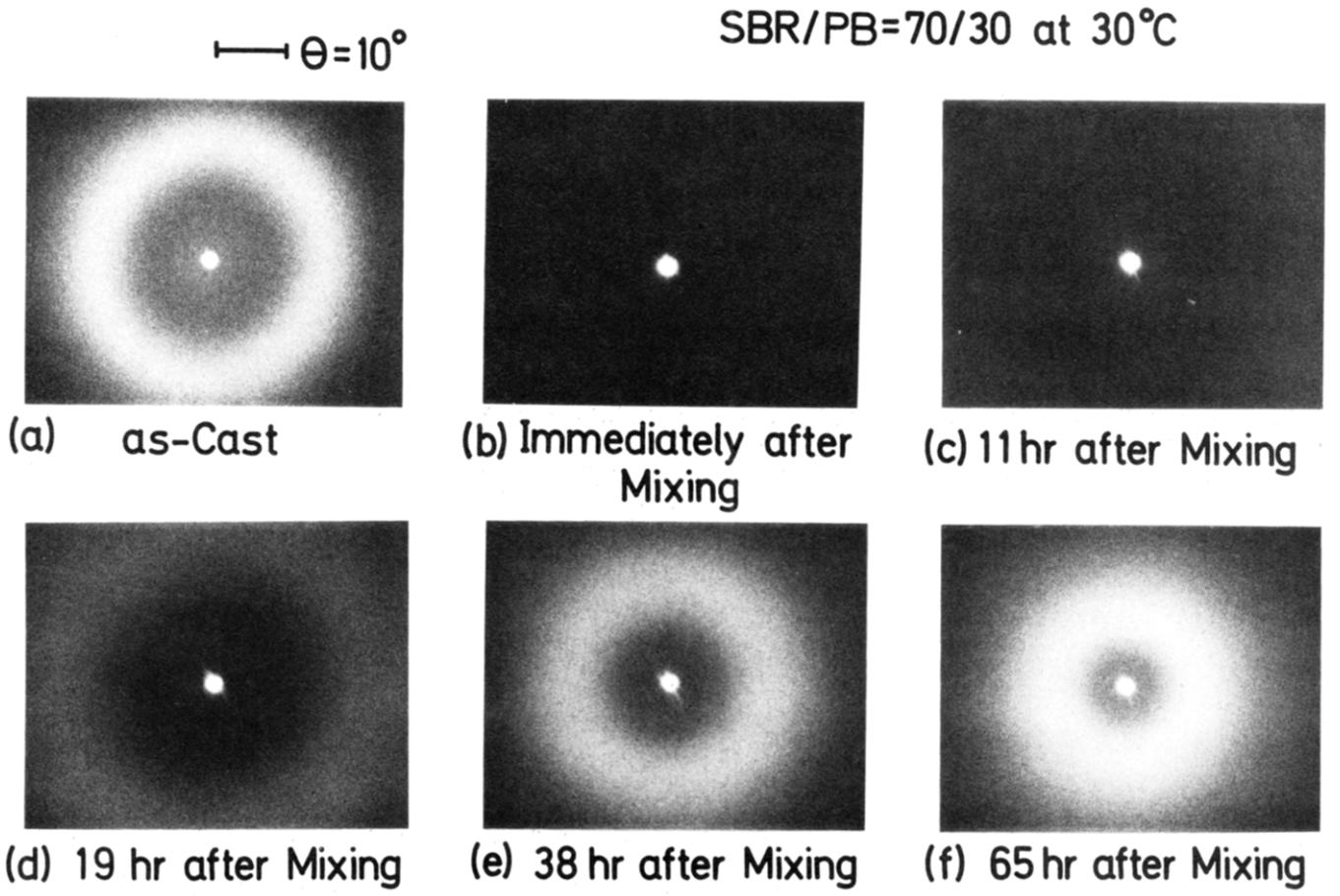

Figure 11. Light-scattering pattern for the as-cast film (a), for the film immediately after homogenization (b), and for the film annealed at 30 °C for 11 (c), 19 (d), 38 (e), and 65 h (f). The angle mark for has the same meaning as in Figure 1. SBR/PB = 70/30 v/v.

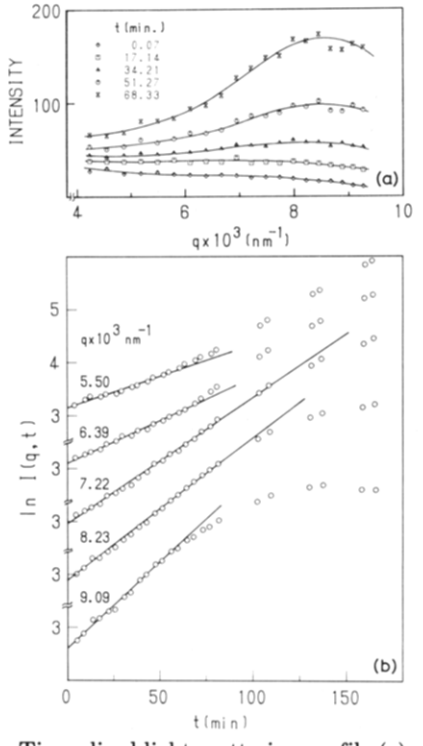

Figure 12. Time-sliced light-scattering profile (a) and change of the scattered intensity with t at various scattering vectors (b) for the early stage spinodal decomposition of 58/42 wt/wt SBR/PB at 60 °C after the homogenization.

of the order of unity. Hence, the phase separation occurs at deep quench, which assures the previous argument associated with eq 8, i.e., $|I_T(q)|$ at $q \ll q_c$, is very small, where q_c is the crossover wavenumber in the Cahn–Hilliard theory[12] at which $R(q) = 0$.

5. Mechanism of Homogenization. The as-cast film or the annealed film has the phase-separated domain structure relevant to the late stage spinodal decomposition. At deep quench, the interface between the two coexisting domains is believed to be sharp and is well defined. The dominant Fourier mode of the concentration fluctuations with wavelength Λ_0 exists in all directions, with equal probability in the undeformed sample. For simplicity let us consider here the Fourier modes of the fluctuations parallel and perpendicular to the compression axis as shown schematically in Figure 15a.

Now let us consider the case in which we applied the $^1/_2$ compression n times to the original film. If the deformation causes simple isochoric affine deformation and the wavelengths of the dominant modes of the fluctuations also are affinely deformed, being contracted to Λ_2 and expanded to Λ_1 in the directions parallel and perpendicular to the compression axis, respectively,

$$\Lambda_2 = \Lambda_0(1/2)^n \qquad \Lambda_1 = 2^{n/2}\Lambda_0 \tag{18}$$

then the gradient free energy $\kappa(\nabla\phi)^2$ in the Ginzburg–Landau[21] and Cahn–Hilliard[12] theories becomes increasingly high and low with n in the directions parallel and perpendicular to the compression axis, respectively. Note that Λ_0 goes to about $\Lambda_2 = 10$ Å, if $n = 10$, and $\Lambda_0 = 1$ μm as encountered in the ordinary experimental situations. Thus, the simple affine deformation during 10 repetitions of the $^1/_2$ compression brings the systems into a state with a very high gradient free energy or causes the fluctuations

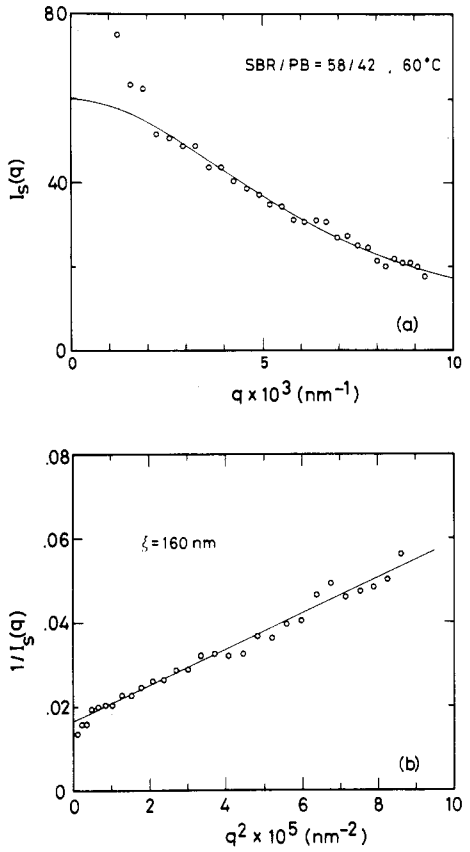

Figure 13. Light-scattering profile $I_s(q)$ for the homogenized film of 58/42 wt/wt SBR/PB at 60 °C (a) and corresponding Ornstein–Zernike plot (b). The solid lines show the best-fit profiles with the Ornstein–Zernike equation with ξ = 160 nm.

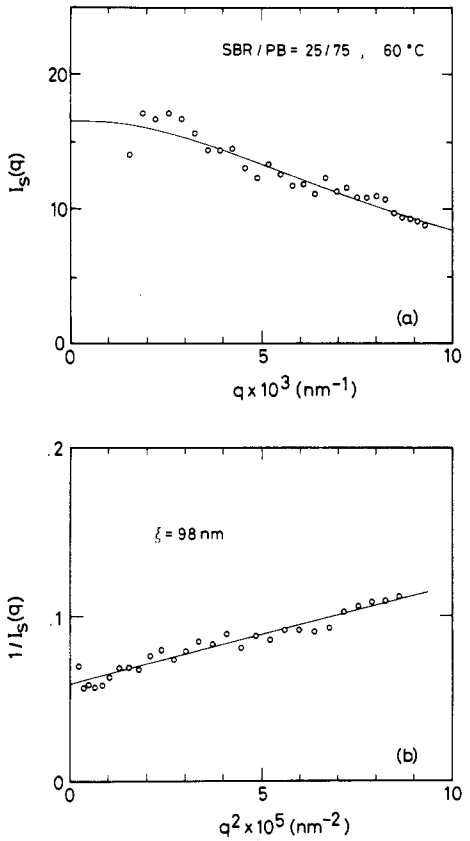

Figure 14. Light-scattering profile $I_s(q)$ for the homogenized film of 25/75 wt/wt SBR/PB at 60 °C and corresponding Ornstein–Zernike plot (b). The solid lines show the best-fit profiles with the OZ equation with ξ = 98 nm. SBR/PB = 25/75 wt/wt.

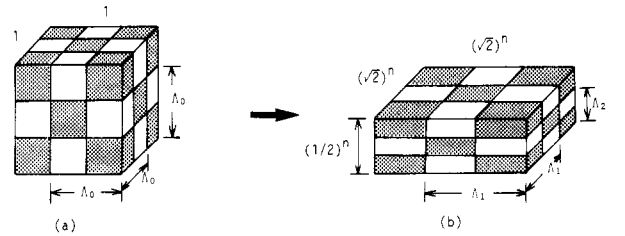

Figure 15. Schematic illustration of the Fourier modes of concentration fluctuations parallel and perpendicular to the compression axis (vertical direction of the figure). (a) Undeformed specimen and (b) specimen subjected by the $^1/_2$ compression n times.

with a high q, much higher than the crossover wavenumber[12] q_c.

Such thermodynamically unfavorable situations as induced by the simple affine deformation described above would not happen in a real system. Instead, the dissolution of the fluctuations with high q values should result in suppression of $\langle \eta^2 \rangle$ as seen in the decrease of the scattered intensity in Figure 7d and also in Figures 9 and 10, in addition to the expansion and contraction of the wavelength of the dominant mode of the fluctuations induced by the simple affine deformation. The mode of the fluctuations, which is forced to have a q value higher than the critical value q_c, will be dissolved and suppressed to the level of the critical fluctuations. The dissolution of the fluctuations which prevails in the direction of the uniaxial compression may also cause the dissolution of the fluctuations occurring in the direction perpendicular to the compression axis due to a nonlinear effect involving mode–mode couplings.

Acknowledgment. This work was supported in part by a Grant-in-Aid for Scientific Research (63470090) and by a Grant-in-Aid for Scientific Research on Priority Areas "New Functionality Materials Design, Preparation and Control" (63604558), both from the Ministry of Education, Science and Culture, Japan, and by a Scientific grant from the Yokohama Rubber Co., Ltd., Japan.

References and Notes

(1) Hashimoto, T.; Sasaki, K.; Kawai, H. *Macromolecules* **1984**, *17*, 2812. Sasaki, K.; Hashimoto, T. *Macromolecules* **1984**, *17*, 2818.
(2) Inoue, T.; Ougizawa, T.; Yasuda, O., Miyasaka, K. *Macromolecules* **1985**, *18*, 57.
(3) Hashimoto, T.; Kumaki, J.; Kawai, H. *Macromolecules* **1983**, *16*, 641.
(4) See for example: Gunton, J. D.; San Miguel, M.; Sahni, P. S. In *Phase Transitions and Critical Phenomena*; Domb, C., Lebowitz, J. L., Eds.; Academic Press: New York, 1983; Vol. 8.
(5) For a review in polymer, see for example: Hashimoto, T. *Phase Transitions* **1988**, *12*, 47.
(6) Hashimoto, T.; Itakura, M.; Hasegawa, H. *J. Chem. Phys.* **1986**, *85*, 6118. Hashimoto, T.; Itakura, M.; Shimidzu, N. *J. Chem. Phys.* **1986**, *85*, 6773.
(7) Izumitani, T.; Hashimoto, T. *J. Chem. Phys.* **1985**, *83*, 3694.
(8) Takenaka, M.; Izumitani, T.; Hashimoto, T. *Macromolecules* **1987**, *20*, 2257.
(9) Izumitani, T.; Takenaka, M.; Hashimoto, T. to be submitted for publication.
(10) Binder, K.; Stauffer, D. *Phys. Rev. Lett.* **1974**, *33*, 1006. Binder, K. *Phys. Rev. B: Solid State* **1977**, *B15*, 4425.
(11) Furukawa, H. *Prog. Theor. Phys.* **1978**, *59*, 1072; *Phys. Rev. Lett.* **1979**, *43*, 136; *Physica A (Amsterdam)* **1984**, *123*, 497.
(12) Cahn, J. W.; Hilliard, J. E. *J. Chem. Phys.* **1959**, *31*, 688. Cahn, J. W. *J. Chem. Phys.* **1965**, *42*, 93.
(13) Cook, H. E. *Acta Metall.* **1970**, *18*, 297.
(14) Binder, K. *J. Chem. Phys.* **1983**, *79*, 6387. Strobl, G. R. *Macromolecules* **1985**, *18*, 558.

(15) Okada, M.; Han, C. C. *J. Chem. Phys.* **1986**, *85*, 5317.
(16) See for example: de Gennes, P. G. *Scaling Concepts in Polymer Physics*; Cornell University: Ithaca, 1979.
(17) Mori, K.; Tanaka, H.; Hashimoto, T. *Macromolecules* **1987**, *20*, 381.
(18) Roe, R. J.; Zin, C. W. *Macromolecules* **1980**, *13*, 1221.
(19) Ornstein, L. S.; Zernike, F. *Proc. Akad. Sci. Amsterdam* **1914**, *17*, 793.
(20) See for example: Stanley, H. E. *Introduction to Phase Transitions and Critical Phenomena*; Oxford, 1971.
(21) See for example: Ma, S. K. *Modern Theory of Critical Phenomena*; Benjamin, 1976.
(22) The temperature of 60 °C was chosen for the isothermal demixing process, because the rate of spinodal decomposition and subsequent coarsening processes occur sufficiently slow, which makes it easy to control the initial condition for the concentration fluctuations for the subsequent experiment on the uniaxial compression. Needless to say, the wavelength of the dominant mode of the fluctuations depends on time as well as temperature.[5]

Free Volume and Physical Aging of Poly(vinyl acetate) Studied by Positron Annihilation

Y. Kobayashi,*,†,§ W. Zheng,‡,§ E. F. Meyer,§ J. D. McGervey,§ A. M. Jamieson,‖ and R. Simha‖

Departments of Physics and Macromolecular Science, Case Western Reserve University, Cleveland, Ohio 44106. *Received August 30, 1988; Revised Manuscript Received November 8, 1988*

ABSTRACT: The positron lifetime technique was used to study the free-volume properties of poly(vinyl acetate) (PVAc) in the liquid and the glass as a function of temperature and aging time. The average hole volume $\langle v_f \rangle$ at each temperature was determined from the orthopositronium (o-Ps) lifetime τ_3 by using an equation of Nakanishi, based on a theoretical model of Tao. The temperature dependence of the product of the intensity of the o-Ps component I_3 and $\langle v_f \rangle$ agrees well with the free-volume fraction h computed from equation-of-state data via the statistical mechanical theory of Simha and Somcynsky. This observation suggests that I_3 is a measure of the number of holes in a polymer matrix. Changes in I_3 during physical aging were found to be proportionately greater than changes in τ_3, in agreement with previous studies. The results indicate that positron annihilation can be a reliable method for monitoring not only free-volume changes but also changes in the distribution of free-volume elements in polymers.

1. Introduction

Physical aging of an amorphous polymer refers to a progressive change of its properties without the intervention of chemical agents. This process occurs in the glassy state, having its origin in the nonequilibrium character of this state and the consequent relaxation toward equilibrium.[1] A convenient phenomenological description can be developed within the classical free-volume concept. The distance from equilibrium can be related to the excess free volume of the glass, and the aging rate can be related to the time evolution of the free-volume distribution. Classical aging experiments have involved well-specified temperature jumps with subsequent observations of macroscopic quantities such as volume, enthalpy, or mechanical properties such as stress relaxation.

The statistical mechanical theory of Simha and Somcynsky[2] provides a powerful vehicle for correlating and predicting aging effects on different materials. The thermodynamic properties of the bulk polymeric state are expressed in terms of a free-volume function, h. However, numerical evaluation of this quantity requires P-V-T information as a function of thermal and pressure history of the specimen under study.[3,4] A more convenient application of the theory as an analytical tool requires a more direct and rapid means of numerically determining h.

Positrons have been successfully used for materials research since it was discovered in the late 1960s that the positron lifetime in a variety of materials is extremely sensitive to phase transitions and to the presence of defects and other inhomogeneities. The utility of positrons in polymer studies is enhanced by the fact that the positron can capture an electron and form a bound system, an atom of positronium (Ps).[5,6] Ps has an atomic radius similar to hydrogen, except that it rapidly decays by positron–electron annihilation. Orthopositronium (o-Ps), where the spins of the two particles are parallel, has a mean lifetime of 142 ns under vacuum. Parapositronium (p-Ps), where the spins of the two particles are antiparallel, has a mean lifetime of only 123 ps. The difference in the o-Ps and p-Ps lifetimes under vacuum is due to the fact that, to conserve spin angular momentum, o-Ps (spin = 1) must produce three photons upon annihilation while p-Ps (spin = 0) only produces two. In condensed matter, the o-Ps lifetime is shortened to a few nanoseconds or less, because of pickoff of the positron by electrons of antiparallel spin in the surrounding medium. However, this lifetime is considerably longer than that of a free positron in the same medium, because the electron in o-Ps partially shields its positron from those electrons with antiparallel spin, which would annihilate it more rapidly. Because of the relatively long lifetime of o-Ps, its component is well-defined in a lifetime spectrum. Therefore, it is possible to make a rather precise determination of the o-Ps lifetime and its intensity (the fraction of positrons that annihilate as o-Ps).

The other important feature of the o-Ps atom in a polymer is that this species is preferentially trapped or formed in regions of low electron density, or holes. Since the annihilation rate of o-Ps is proportional to the overlap of the positron and the pickoff electron wave functions,[7] it is expected that the o-Ps lifetime will strongly depend upon the size of the hole. Numerous experiments[7-13] have

† Permanent address: National Chemical Laboratory for Industry, Tsukuba, Ibaraki 305, Japan.
‡ Permanent address: Shanghai Institute of Nuclear Research, Academia Sinica, P.O. Box 8204, Shanghai, China.
§ Department of Physics.
‖ Department of Macromolecular Science.

0024-9297/89/2222-2302$01.50/0